

Astrometric Measurements of 05276-0843 HLD 75, 06347-8239 WFC 38, 05445-2058 KPP 125, 10296+3757 HJ 2532 AB and 09174+2339 STF 1332 (HD 79872)

Rishi Janakiraman¹, Siqi Li¹, Marlin S.M. Humphreys¹, Mateus Arruda¹, Xinyue Wang¹, Kalée Tock¹
¹Stanford Online High School, Redwood City, California; rishi.jraman@gmail.com

Abstract

The double star systems 05276-0843 HLD 75, 06347-8239 WFC 38, 05445-2058 KPP 125, 10296+3757 HJ 2532 AB, and 09174+2339 STF 1332 (HD 79872) were measured and analyzed to classify each system as physically related and/or gravitationally bound. Our team requested 10-11 images of each system from the Las Cumbres Observatory Global Telescope network, which were then analyzed in AstroImageJ to compute the average position angle and separation. These were then plotted alongside historical measurements. Only 09174+2339 STF 1332 (HD 79872) showed evidence of a trend in the secondary's position relative to the primary over time, consistent with its known orbital solution. Gaia DR3 measurements on parallax and proper motion showed that all systems were likely physically related, but 05276-0843 HLD 75 had comparably lesser similarity in its component stars' proper motions. Only systems 10296+3757 HJ 2532 AB and 09174+2339 STF 1332 (HD 79872) had relative velocities within their respective computed system escape velocities, supporting their classification as binary systems.

1. Introduction

Double star systems with similar parallax (Plx) and proper motion (PM) can be classified into two broad categories—physical doubles and binary stars. Physical doubles have similar Plx and PMs, suggesting that the stars are physically close together and move together in space. If a physical double is gravitationally bound, it is called a binary system.

Physical doubles are useful because they likely share a common origin, so their behavior can be analyzed to draw inferences on galaxy evolution and to reconstruct events like galaxy mergers. Binaries, on the other hand, orbit a common center of mass, so astronomers can calculate both stars' masses (and thus infer their lifetimes). This paper investigates the likelihood of 5 double star systems' classification as either a physical double or binary system using inferences from archival data combined with new astrometric data.

The systems 05276-0843 HLD 75, 06347-8239 WFC 38, 05445-2058 KPP 125, 10296+3757 HJ 2532 AB, and 09174+2339 STF 1332 (HD 79872) were chosen from the Washington Double Star Catalog (WDS) using the following search constraints: the system must

- a) Have a right ascension (RA) between 5 and 13 hours to be near zenith during January and February, when this study was conducted. Dec was not constrained since the images were accessed through the Las Cumbres Observatory Global Telescope (LCOGT) network, which has telescopes in both hemispheres.
- b) Have a secondary star magnitude < 13 so that the stars in the image are bright enough to be clearly viewable by a 0.35m Delta Rho telescope.
- c) Have a difference in brightness of less than 3 magnitudes so that the pair can be imaged together using the same exposure time.
- d) Have a separation between 5" and 15" so that both stars are resolved on the same image.

- e) Have a listing of “physical” on the Stelle Doppie database so that chosen systems will have similar Plx and PMs.

For the primary and secondary stars of each system, BP-RP colors and G-filter magnitudes were retrieved from the Gaia Data Release 3 (DR3) (Gaia Collaboration, 2023; 2016b; 2023j). The stars’ Gaia G absolute magnitudes (M) were computed using Equation 1. This equation standardizes the effects of parallax on the G-filter magnitudes that were directly retrieved from Gaia DR3.

Figure 1 was used to estimate spectral types by plotting Gaia BP-RP color and Gaia G absolute magnitude (Table 1) for all stars. The Gaia BP-RP color on the x-axis is used as a proxy for surface temperature, while the Gaia G absolute magnitude on the y-axis is used as a proxy for luminosity. Spectral types were estimated by matching the star’s position on Figure 1 to its spectral type marking. All stars were found to be on the main sequence except for 05276-0843 HLD 75’s primary, which is on the red giant branch.

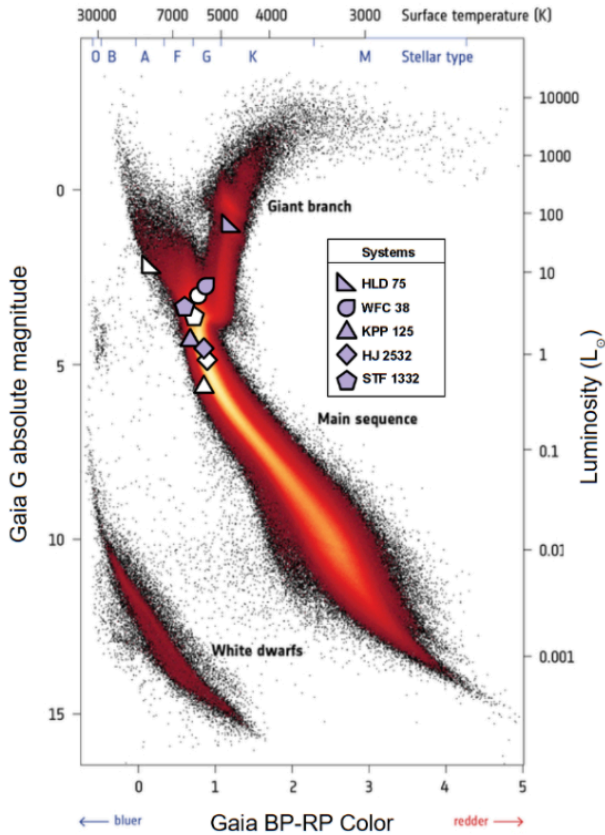


Figure 1: Primary (purple) and Secondary (white) Star of each system plotted on Gaia’s HR Diagram according to BP-RP Color and Gaia G Absolute Magnitude (Gaia Collaboration et al., 2018).

$$M = m + 5 \cdot (\log p + 1)$$

Equation 1: Gaia G absolute magnitude (M) standardizes G-filter magnitude (m) by accounting for parallax (p).



Table 1: Colors and Magnitudes from Gaia DR3 (bolded column headings were plotted on Figure 1’s HR Diagram)

| System | Star | Gaia BP-RP Color | Gaia G-filter Magnitude (m) | Gaia G Absolute Magnitude (M) |
|-----------------------------------|------|-------------------------|---------------------------------|---|
| 05276-0843 HLD 75 | Pri | 1.20 | 9.20 | 1.08 |
| | Sec | 0.64 | 10.42 | 2.30 |
| 06347-8239 WFC 38 | Pri | 0.84 | 11.02 | 3.03 |
| | Sec | 0.80 | 11.13 | 3.16 |
| 05445-2058 KPP 125 | Pri | 0.83 | 11.45 | 4.08 |
| | Sec | 0.99 | 12.92 | 5.48 |
| 10296+3757 HJ 2532 AB | Pri | 0.80 | 10.19 | 4.64 |
| | Sec | 0.83 | 10.40 | 4.86 |
| 09174+2339 STF 1332 (HD 79872) | Pri | 0.60 | 7.83 | 3.47 |
| | Sec | 0.66 | 8.14 | 3.77 |



Table 2 reports the systems’ estimated spectral types from Figure 1, estimated masses, and latest published position angle (PA) and separation (Sep) data retrieved from previous papers on the SIMBAD database (Wegner, 2000). For all systems, spectral type estimations were cross-referenced with the

University of Northern Iowa’s list of spectral type characteristics to estimate masses (Morgan et al., 2023).

Table 2: Basic Information on Systems (retrieved from Gaia DR3) with Spectral Type and Mass Estimates (bolded) and Latest PA/Sep Measurements (retrieved from SIMBAD)

| System | Coordinates HMS:DMS | Star | Spectral Type | Mass (M_{\odot}) | Latest PA/Sep Date | PA | Sep |
|--------------------------------------|-----------------------------|------|--------------------------|--|-------------------------------|-----------|------------|
| 05276-0843 HLD 75 | 05:27:37.74 -08:42:37.20 | Pri | K | 1 | 2018.975 ¹ | 89.1 | 6.248 |
| | | Sec | A4 | 1.8 | | | |
| 06347-8239 WFC 38 | 06:34:43.21 -82:38:38.73 | Pri | G/F | 1 | 2016.0 ² | 3.46 | 5.04738 |
| | | Sec | G/F | 1 | | | |
| 05445-2058 KPP 125 | 05:44:28.12 -20:58:14.78 | Pri | F | 1.2 | 2015.5 ³ | 153.372 | 4.95811 |
| | | Sec | G | 0.9 | | | |
| 10296+3757 HJ 2532 AB | 10:29:35.30 +37:57:29.9 | Pri | G1 | 1.04 | 2016.0 ² | 69.68 | 13.03165 |
| | | Sec | G2 | 1 | | | |
| 09174+2339 STF 1332 (HD 79872) | 09:17:19.21 +23:39:09.8 | Pri | F | 1.3 | 2019.245 ⁴ | 29.413 | 5.9325 |
| | | Sec | F | 1.3 | | | |

¹(Mason et al, 2021)

²(Kareem et al, 2021)

³(Knapp, 2018)

⁴(Izmailov et al., 2020)

Previous papers on 10296+3757 HJ 2532 AB have classified the system as a wide binary using Bayesian analyses based on PM/Plx uncertainties and relative velocity (Andrews et al., 2017). 09174+2339 STF 1332 (HD 79872)’s historical data strongly suggest the system is bound, and has a proposed orbital solution (Izmailov, 2019).

2. Instruments

All systems were imaged using telescopes from the Las Cumbres Observatory (LCOGT) robotic telescope network (Brown, 2013). All systems were measured with the DeltaRho+QHY600 telescope-camera system, which has an aperture of 0.35m and an FOV of 1.9° x 1.2°, which is cut down to 30' x 30' in the default “central mode.” Table 3 shows information about the filters used and the exposure times that each system was imaged with. The Bessel-V (V) filter and Pan-STARRS w (W) filters were both used to image the different systems, as specified in Table 3 (Bessell, 1990; Tonry, J.L. et al, 2012).

Table 3: Filters and Exposure Times for LCOGT Requests

| System | Filter | Exposure Time (s) |
|--------------------------------------|--------|-------------------|
| 05276-0843 HLD 75 | V | 10 |
| 06347-8239 WFC 38 | V | 17 |
| 05445-2058 KPP 125 | W | 20 |
| 10296+3757 HJ 2532 AB | V | 8 |
| 09174+2339 STF 1332 (HD 79872) | V | 1 |

All systems were imaged at the LCOGT observatory in Tenerife, Spain except for 06347-8239 06347-8239 WFC 38, which was imaged at Sutherland, South Africa.

3. Measurements

Images were requested from LCOGT for each system (number of images reported in Table 4). Only 06347-8239 06347-8239 WFC 38 had a compromised image in which the secondary star was measured to be brighter than the primary. This image, pictured in Figure A (Appendix A), was removed from calculations, and all other images resolved well and were included.

In AstroImageJ (AIJ), the multi-aperture photometry tool was used to make measurements of position angle (PA) and separation (Sep) for all systems' requested images. For each system, the average PA/Sep (with standard error) was calculated and reported in Table 4, while the full list of individual observations can be found in Table A (Appendix A). An example of an AIJ measurement for each system is shown in Figure 2.

Table 4: AIJ Measurements for Each System, Including Average PA/Sep with Error

| System | Julian Date | Number of Images | Aperture Radius (px) | Avg PA (°) ± SE | Avg Sep (") ± SE |
|-----------------------|-------------|------------------|----------------------|-----------------|------------------|
| 05276-0843 HLD 75 | 2024.019 | 11 | 4.0 | 89.1 ± 0.02 | 6.27 ± 0.005 |
| 06347-8239 WFC 38 | 2025.033 | 9 | 3.5 | 3.8 ± 0.11 | 5.16 ± 0.039 |
| 05445-2058 KPP 125 | 2025.030 | 10 | 3.2 | 154.0 ± 0.27 | 4.99 ± 0.048 |
| 10296+3757 | 2025.038 | 10 | 7.0 | 69.7 ± 0.02 | 13.03 ± 0.010 |

| | | | | | |
|--------------------------------------|----------|----|-----|-----------------|------------------|
| HJ 2532 AB | | | | | |
| 09174+2339 STF 1332 (HD 79872) | 2025.041 | 10 | 3.0 | 29.6 ± 0.16 | 5.90 ± 0.031 |

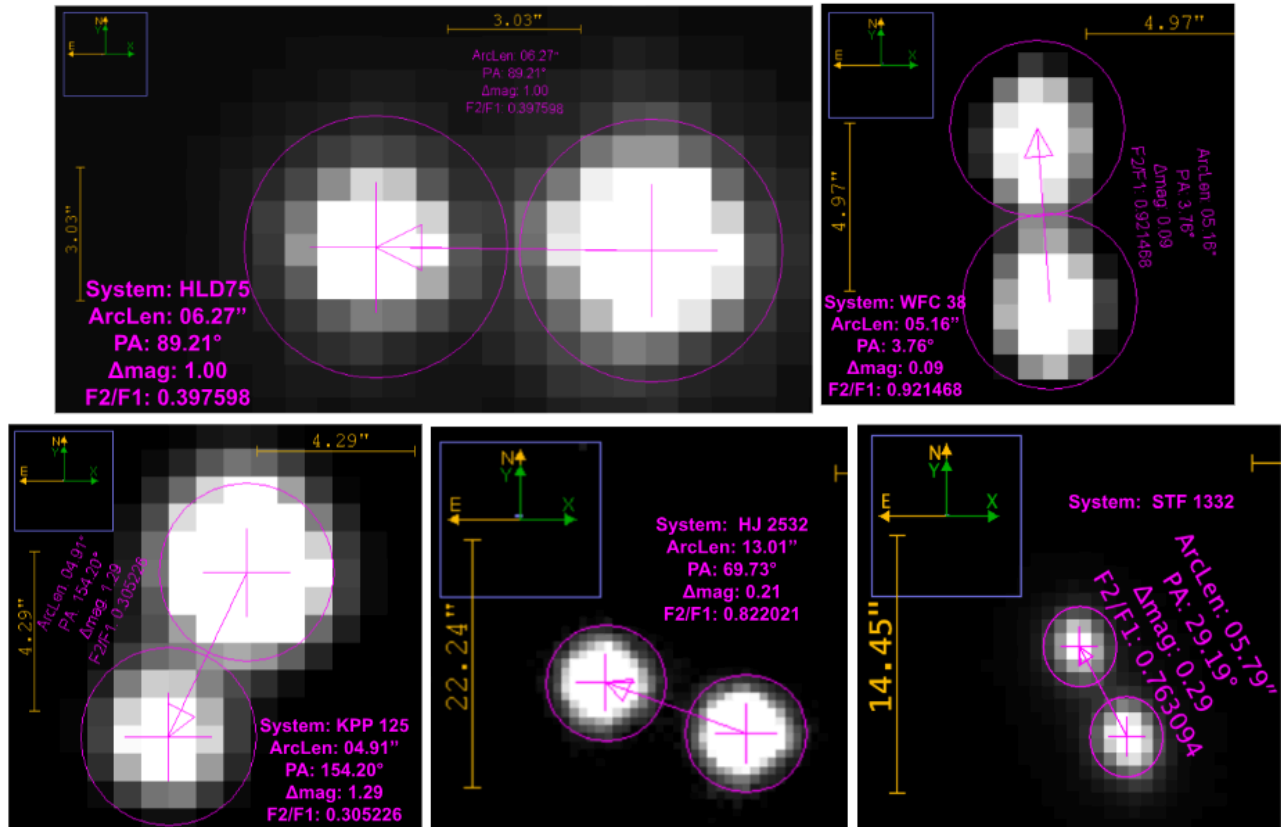


Figure 2: Sample measurement screenshots. From left to right: 05276-0843 HLD 75, 06347-8239 06347-8239 WFC 38, 05445-2058 KPP 125, 10296+3757 HJ 2532 AB, and 09174+2339 STF 1332 (HD 79872)

4. Results

In Table 5, data retrieved from the Gaia DR3 are reported, which include parallax with uncertainty, PM RA/Dec, and the relative velocities of both stars in each system.

Using Gaia DR3 PM RA and PM Dec (Table 5) as component vectors, the *individual* PM vector magnitudes for each system's two stars are calculated. The difference vector between these two is known as the relative PM vector, whose magnitude is reported in Table 5. The relative PM vector magnitude and the magnitude of the longer individual PM vector were used to calculate the ratio of proper motion (rPM) in the final column according to Equation 2.

$$\text{rPM} = \frac{\|\mathbf{u} - \mathbf{v}\|}{\|\mathbf{v}\|}$$

Equation 2: The equation for the ratio of proper motion (rPM), in which vectors u and v are PM vectors, one for each star in the double. In this case, vector v is the longer of the two. The difference vector between u and v is known as the relative PM vector.

The quotient between the relative PM vector's magnitude and the magnitude of the longer individual PM vector is known as rPM (Equation 2). Thus, a low rPM quotient means that the motion of the secondary star—relative to the primary—is small with respect to the overall motion of the system. Therefore, a small rPM indicates that the stars are moving similarly and are likely physically related. The range for common PM (CPM)—the most physically related category—is an rPM of 0 to 0.2, which all systems except 05276-0843 HLD 75 fall under (Harshaw, 2016). 05276-0843 HLD 75 is only 0.02 above that threshold.

Table 5: Gaia DR3 Parallax and Proper Motion Measurements with Relative Proper Motions (bolded columns are calculated values)

| System | Star | Parallax (mas) ± Uncertainty | PM RA (mas/yr) | PM Dec (mas/yr) | Radial velocity (m/s) | Relative PM vector mag (mas/yr) | rPM |
|--------------------------------------|------|------------------------------|----------------|-----------------|-----------------------|--|------------|
| 05276-0843 HLD 75 | Pri | 2.379 ± 0.015 | 2.17262 | 2.12434 | 52323 | 0.67 | 0.22 |
| | Sec | 2.378 ± 0.076 | 1.52482 | 1.96235 | 53147 | | |
| 06347-8239 WFC 38 | Pri | 2.534 ± 0.011 | -2.0955 | -10.2986 | -911 | 0.28 | 0.03 |
| | Sec | 2.547 ± 0.012 | -1.8375 | -10.4191 | 2994 | | |
| 05445-2058 KPP 125 | Pri | 3.350 ± 0.136 | 8.3217 | 24.3443 | 47239 | 1.80 | 0.07 |
| | Sec | 3.249 ± 0.014 | 8.9353 | 22.6532 | 48698 | | |
| 10296+3757 HJ 2532 AB | Pri | 7.768 ± 0.023 | 62.8927 | -51.0016 | -19637 | 0.24 | 0.03 |
| | Sec | 7.791 ± 0.024 | 62.6711 | -50.9163 | -19044 | | |
| 09174+2339 STF 1332 (HD 79872) | Pri | 13.388 ± 0.032 | -47.9634 | -65.5841 | 18871 | 6.64 | 0.08 |
| | Sec | 13.380 ± 0.036 | -41.7044 | -67.8028 | N/A | | |

To suggest gravitational binding, the system escape velocity and relative 3D space velocity were compared.

For a double-star system, the system escape velocity is the minimum speed an object must have to escape both stars' gravitational pull, and it is calculated with Equation 3 (Bonifacio et al., 2020):

$$v_e = \sqrt{\frac{2G(M_p + M_s)}{R}}$$

Equation 3: The equation for escape velocity (v_e) given the gravitational constant (G), the masses of the primary and secondary stars (M_p and M_s), and the distance between them (R).

In Equation 3 for system escape velocity, the distance R would normally account for both 1) the transverse separation *in space*, which is the physical distance between the primary and secondary perpendicular to our line of sight, and 2) the radial separation between the primary and secondary parallel to our line of sight. However, since the parallax uncertainties overlap for all systems (Table 5), we assume that the primary and secondary have no radial separation, and thus substitute the in-space transverse separation for R. Equation 4 describes the formula for in-space transverse sep, which incorporates the latest published separation (Table 1) and the parallax of the system (Table 5).

$$R = Sep_{pc} = \frac{Sep_{arcseconds} \cdot \frac{1^\circ}{3600''} \cdot \frac{2\pi \text{ radians}}{360^\circ}}{Plx''}$$

Equation 4: In-space transverse Sep (substituted as R in Equation 3) incorporates the latest Sep measurement ($Sep_{arcseconds}$) and the parallax (Plx'') to yield the physical transverse Sep in pc.

Another metric reported in Table 6 is relative 3D space velocity, which incorporates both relative transverse and relative radial velocity into one value via Euclidean norm. Relative transverse velocity uses the small angle tangent approximation to convert the relative PM vector magnitude (Table 5) from mas/year to m/s. Relative radial velocity is the absolute difference between the radial velocity of the primary and secondary, both of which were reported in Table 5. 09174+2339 STF 1332 (HD 79872) did not have a secondary radial velocity measured by Gaia DR3, so its relative radial velocity was assumed to be 0 m/s.

Thus, relative 3D space velocity measures the stars' motion relative to one another in 3D space. If the relative 3D space velocity exceeds the escape velocity, the stars have enough kinetic energy to overcome the gravitational pull between them. In this case, they would be moving too fast to remain bound and would eventually drift apart.

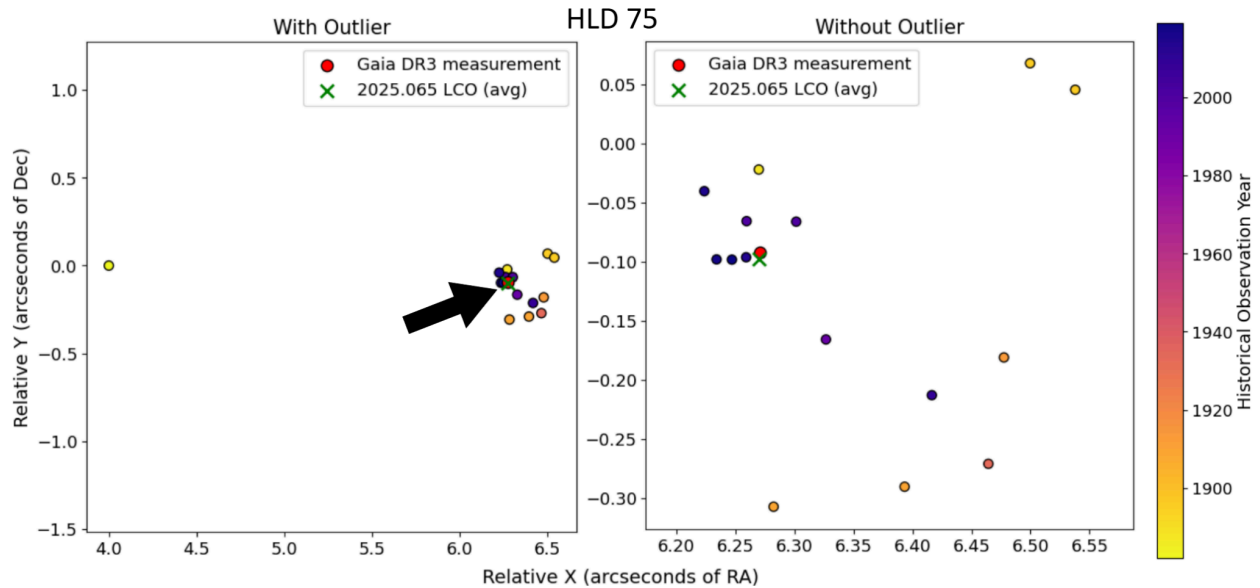
Table 6: Comparison of System Escape Velocity with Relative 3D Velocity (both bolded)

| System | System Escape velocity (m/s) | Relative 3D velocity (m/s) |
|--------------------------------------|-------------------------------------|-----------------------------------|
| 05276-0843 HLD 75 | 1376 | 1565 |
| 06347-8239 WFC 38 | 1334.79 | 3942 |
| 05445-2058 KPP 125 | 1549 | 2934 |
| 10296+3757 HJ 2532 AB | 1471 | 610 |
| 09174+2339 STF 1332 (HD 79872) | 3475 | 2351 |

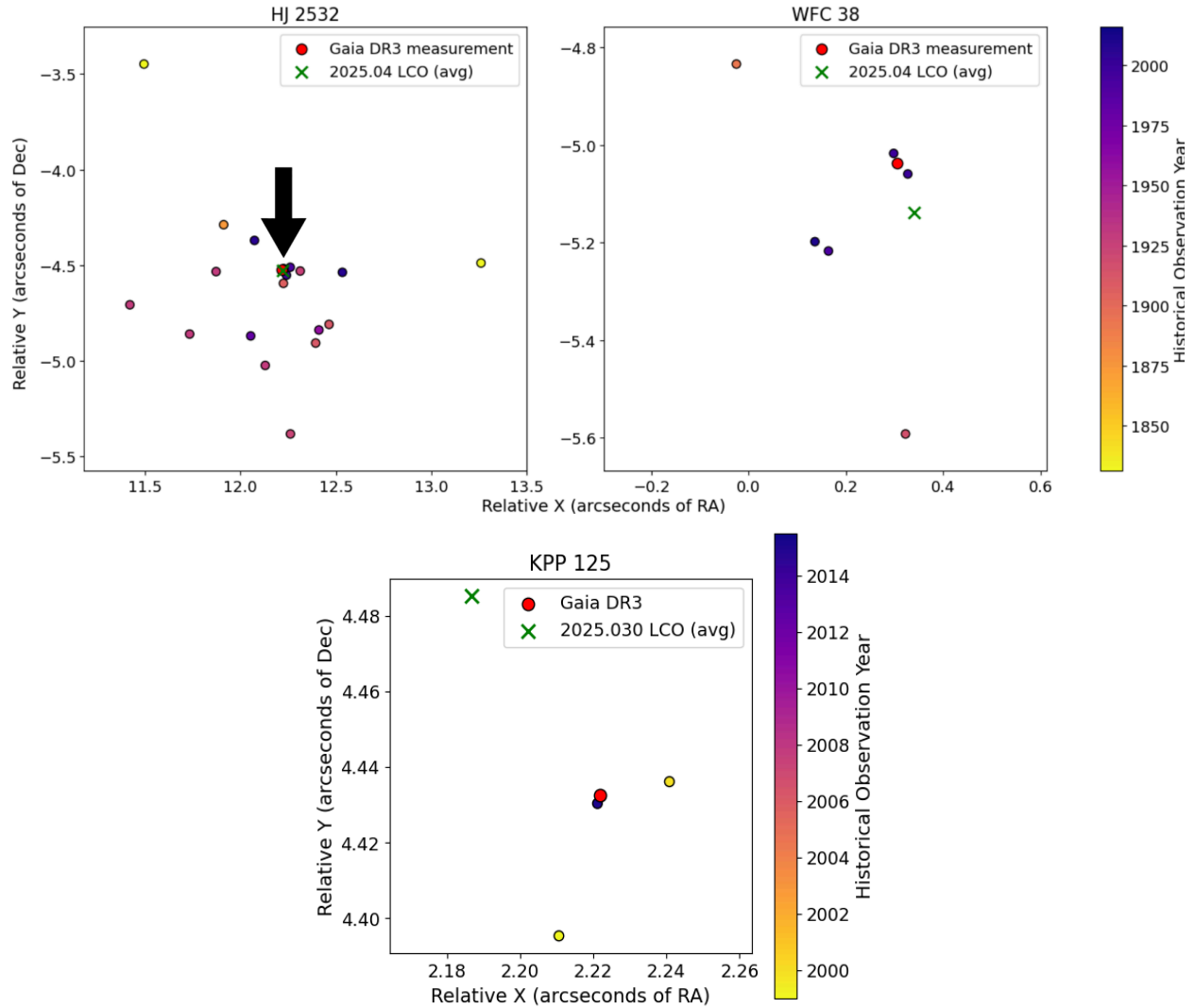
The two bolded columns of Table 6 compare the system escape velocity (m/s) to the relative 3D space velocity (m/s). For systems 05276-0843 HLD 75, 06347-8239 WFC 38, and 05445-2058 KPP 125, the relative 3D velocity exceeds the system escape velocity, which suggests that they are not gravitationally bound. On the other hand, systems 10296+3757 HJ 2532 AB and 09174+2339 STF 1332 (HD 79872) both have a relative 3D velocity lower than the system escape velocity, which suggests that they are both gravitationally bound.

5. Plots

Figures 3a-e show historical measurements of the secondary star’s position in RA and Dec relative to the primary (represented by the origin) for all systems except 09174+2339 STF 1332 (HD 79872), which is in Figure 4. These positions were obtained by transforming the historical PA/Sep into relative positions. On all figures, the Gaia DR3 measurement is represented by a red circle, while the measurement made by this study is represented by a green “X”. Figure 3a likely has an outlier, as its 1884 measurement has an RA of 4" (Holden, 1882). Figure 3b plots the data with the outlier excluded and the axes scaled accordingly.



Figures 3a-b: Left: Relative position of the secondary star with respect to the primary of 05276-0843 HLD 75 (outlier included). Right: Figure 3a with outlier excluded.



Figures 3c-e: Left to Right: Relative position of the secondary star with respect to the primary of 10296+3757 HJ 2532 AB, 06347-8239 WFC 38 and 05445-2058 KPP 125

While its earlier, yellow-color mapped observations show scatter, Figure 3b’s more recent measurements show a minor trend in the secondary star’s relative position over temporal progression. Since few observations are this recent (post-2015), though, there is not enough data to extrapolate a larger relationship between the secondary and primary stars. Both 06347-8239 WFC 38 and 05445-2058 KPP 125 (Figures 3d and 3e) lack the amount of data required to evidence a trend over time in the data ($n = 10$; $n = 5$). Similarly, the scatter in 10296+3757 HJ 2532 AB (Figure 3c) precludes any inference of a trend over time in relative position.

Since it had an orbital solution, 09174+2339 STF 1332 (HD 79872) was plotted separately in Figure 4 alongside its orbital solution (retrieved from SIMBAD) and the predicted point from the orbital solution was plotted alongside historical data (Izmailov, 2019). Below, Figure 4a shows both the historical data plot for 09174+2339 STF 1332 (HD 79872) and its orbital solution. Figure 4b shows the orbital solution’s predicted point superimposed on the historical data plot.

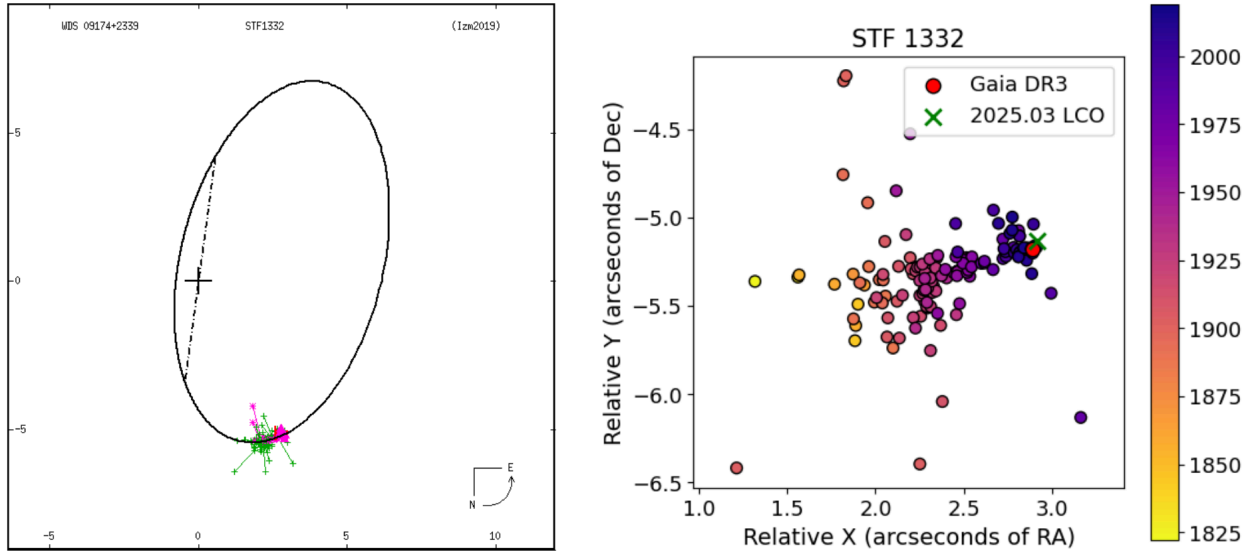


Figure 4a: Left: proposed orbital solution for 09174+2339 STF 1332 (HD 79872) (Izmailov, 2019). Right: Plot of the secondary star position relative to the primary.

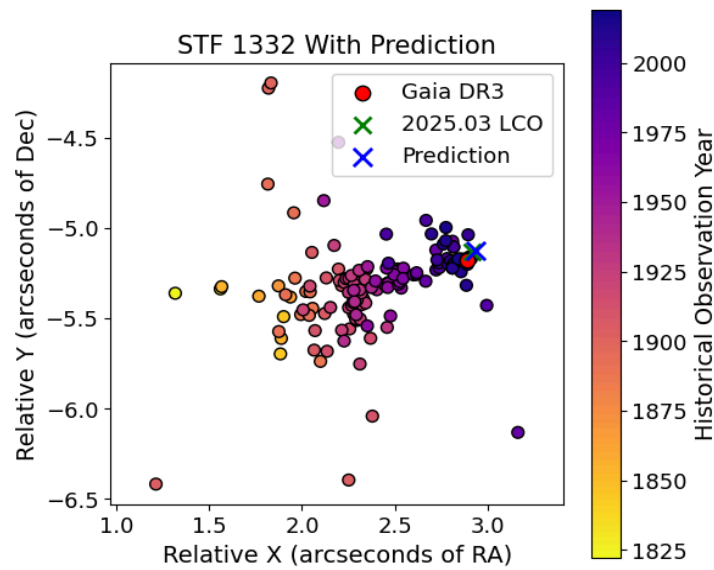


Figure 4b: Historical data plot for 09174+2339 STF 1332 (HD 79872) with the blue "X" representing the orbital solution's prediction for 2025.00.

As seen in Figure 4b, the predicted point from the proposed orbital solution aligns with this study's measurement.

6. Discussion

For all 5 systems, the Gaia DR3 measurements plotted within 1" to this study's measurements (Figures 3 and 4), which indicates that the PA/Sep measurements presented here were accurate. As for historical data, the trend varied depending on the system. 05276-0843 HLD 75's historical data (Figure 3a) showed scatter in earlier measurements, but recent observations (namely four of them) display a trend over time in the secondary star's position relative to the primary. While this is notable, the recency of the trend

(post-2015) and lack of trend-following observations reduces how confident we can be in our inference. We cannot confidently extrapolate this trend to future measurements.

09174+2339 STF 1332 (HD 79872) has a known orbital solution (Izmailov, 2019) and the greatest number of observations. In Figure 4a, there is evidence to cite a trend over time, with more recent measurements having a greater RA and Dec for the secondary relative to the primary. The orbital solution's prediction for the relative position of the secondary star plots within 0.25 arcseconds of this study's measurement. A summary of inferences made from the historical plots is presented in the third column of Table 7.

In terms of quantitative inferences, we used three major points of comparison to determine whether the double was physical or a binary: 1) parallax similarity 2) rPM and 3) a comparison between relative 3D space velocity and escape velocity.

In all 5 systems, the range of potential parallaxes for the primary and secondary overlap, which makes it possible that the two stars in each system have a radial separation of effectively 0 (Table 5). For four of the star systems, the rPM (Table 5), was below 0.2 by nearly an order of magnitude, suggesting that they have common proper motion through space. The system 05276-0843 HLD 75 has an rPM 0.02 above 0.2, which suggests a similar, but overall not shared proper motion through space (Harshaw 2016).

Table 6 suggests that 05276-0843 HLD 75, 06347-8239 WFC 38, and 05445-2058 KPP 125 are gravitationally unbound, while 10296+3757 HJ 2532 AB and 09174+2339 STF 1332 (HD 79872) are both likely bound. The main point of evidence was the greater escape velocity when compared to relative 3D velocity for the bound-predicted systems. While the large uncertainties in how the masses were found for each star could affect the escape velocity, they are unlikely to change the verdict due to significant divergences between relative 3D velocity and escape velocity for all 5 systems. For 09174+2339 STF 1332 (HD 79872), the additional visible historical trend over time in the secondary star's relative position (Figure 4) provides the strongest evidence that its stars are bound out of all systems. Quantitative inferences are presented as well in Table 7 below.

Table 7: Historical Plot & Quantitative Data Inferences

| System | Number of measurements (n) | Historical plot inferences | PM Type | Which is greater? Escape vs. Relative Velocity | Verdict |
|--------------------------|----------------------------|---|-------------------------|--|---------|
| 05276-0843 HLD 75 | 20 | Possible trend in recent data, still needs more supporting observations | Not common, but similar | Relative velocity | Unbound |
| 06347-8239 WFC 38 | 10 | Too few observations to infer a trend | Common | Relative velocity | Unbound |
| 05445-2058 KPP 125 | 5 | Too few observations to infer a trend | Common | Relative velocity | Unbound |
| 10296+3757 HJ 2532 AB | 27 | Historical data too scattered to infer a trend | Common | Escape velocity | Bound |

| | | | | | |
|--------------------------------------|-----|--|--------|-----------------|-------|
| 09174+2339 STF 1332 (HD 79872) | 146 | Trend over time; current measurement agrees with the existing orbital solution | Common | Escape velocity | Bound |
|--------------------------------------|-----|--|--------|-----------------|-------|

7. Conclusion

Each of the system's measurements align with data from Gaia's DR3 and fall within the uncertainty of the scatter in the historical data plots. 05276-0843 HLD 75 was found to be unlikely to be physically related ($r_{PM} > 0.2$), but its overlapping parallax uncertainties and similar PMs suggest otherwise. 06347-8239 WFC 38 and 05445-2058 KPP 125 have low r_{PM} values (< 0.2), suggesting a stronger likelihood of a physical relationship, however, both their relative 3D velocities exceed their system escape velocities and the systems' lack of historical data deter classifying them as gravitationally bound. Finally, 10296+3757 HJ 2532 AB's and 09174+2339 STF 1332 (HD 79872)'s relative 3D velocities do not exceed their system escape velocities, strongly suggesting that the systems are gravitationally bound. In particular, this study's measurement of 09174+2339 STF 1332 (HD 79872) is within 0.25 arcseconds of the prediction from the system's existing orbital solution.

Acknowledgments

This research has made use of the Washington Double Star Catalog maintained at the U.S. Naval Observatory. This research has made use of the Stelledoppie (www.stelledoppie.it) catalog maintained by Gianluca Sordiglioni. This research has made use of the AstroImageJ software which was written by Karen Collins and John Kielkopf. This research has made use of the SIMBAD database, operated at CDS, Strasbourg, France (Wenger et al. 2000).

This work has made use of data from the European Space Agency (ESA) mission Gaia (<https://www.cosmos.esa.int/gaia>), processed by the Gaia Data Processing and Analysis Consortium (DPAC, <https://www.cosmos.esa.int/web/gaia/dpac/consortium>). Funding for the DPAC has been provided by national institutions, in particular, the institutions participating in the Gaia Multilateral Agreement.

This work makes use of observations taken by the Planewave Delta Rho 350 + QHY600 CMOS camera systems of Las Cumbres Observatory Global Telescope Network located in Tenerife, Spain. This work makes use of observations made with the QHY600 instrument at SAAO in Sutherland, South Africa, operated by the Las Cumbres Observatory.

This research has made use of the Stellarium planetarium. Plots were made using Google Colab and the matplotlib library.

References

- Andrews J. J., J. Chanamé, M. A. Agüeros (2017). Wide binaries in Tycho-Gaia: search method and the distribution of orbital separations. *Monthly Notices of the Royal Astronomical Society*. 472(1), 675–699. Issue 1, November 2017, Pages 675–699. Retrieved from <https://academic.oup.com/mnras/article/472/1/675/4064384>
- Bessell, M. S (1990). UBVRI Passbands. *Publications of the Astronomical Society of the Pacific*, 102, 1181-1199. Retrieved from <https://adsabs.harvard.edu/full/1990PASP..102.1181B>

- Bonifacio, B., C. Marchetti, R. Caputo, et al. (2020). Measurements of Neglected Double Stars. *Journal of Double Star Observations*, 16(5), 411–423. Retrieved from http://www.jdso.org/volume16/number5/Bonifacio_411_423.pdf
- Brown, T. M. et al. (2013). Las Cumbres Observatory Global Telescope Network. *Publications of the Astronomical Society of the Pacific*, 125(931), 1031–1055. Retrieved from <https://iopscience.iop.org/article/10.1086/673168/meta>
- Gaia Collaboration, T. Prusti, J.H.J. de Bruijne, et al. (2016b). The Gaia mission. *A&A* 595, A1. Retrieved from https://www.aanda.org/articles/aa/full_html/2016/11/aa29272-16/aa29272-16.html
- Gaia Collaboration, A. Vallenari, A. G. A. Brown, et al. (2023j). Gaia Data Release 3. Summary of the content and survey properties. *A&A* 674, pp. A1. Retrieved from <https://arxiv.org/abs/2208.00211>
- Harshaw, Richard (2016). CCD Measurements of 141 Proper Motion Stars: The Autumn 2015 Observing Program at the Brilliant Sky Observatory, Part 3. *Journal of Double Star Observations*, 12(4), 394–399. Retrieved from http://www.jdso.org/volume12/number4/Harshaw_394_399.pdf
- Holden, E.S. (1882). Washburn Observatory, I. *Publications of the Washburn Observatory of the University of Wisconsin*, 1, 77.
- Izmailov, I. S. (2019). The Orbits of 451 Wide Visual Double Stars. *Astronomy Letters*, 45, 30-38. Retrieved from <https://doi.org/10.1134/S106377371901002X>
- Izmailov I, Rublevsky A, Apetyan A (2020). Astrometric observations of visual binaries using 26-inch refractor at Pulkovo Observatory during 2014–2019. *Astronomisch Nachrichten*.341: 762–769. Retrieved from <https://doi.org/10.1002/asna.202013815>
- Kareem El-Badry, Hans-Walter Rix, Tyler M Heintz (2021). A million binaries from Gaia eDR3: sample selection and validation of Gaia parallax uncertainties. *Monthly Notices of the Royal Astronomical Society*, 506(2), 2269–2295. Retrieved from <https://academic.oup.com/mnras/article/506/2/2269/6131876>
- Knapp, W. R. A. (2018). Jonckheere Double Star Photometry – Part VIII: Sextans. *Journal of Double Star Observations*, 14(1), 59-65. Retrieved from <http://www.jdso.org/volume14/number1/January2018IssueB.pdf>
- Mason, B. D., Williams, S. J., Matson, R. A., et al. (2021). VizieR Online Data Catalog: Speckle interferometry at the USNO. XXIV. (Mason+, 2021). *The Astronomical Journal*, 162(2). Retrieved from <https://iopscience.iop.org/article/10.3847/1538-3881/abfaa2>
- Morgan, Siobahn (2023). Spectral Type Characteristics. Retrieved Feb, 2025 from <https://sites.uni.edu/morgans/astro/course/Notes/section2/spectralmasses.html>
- Tonry, J.L. et al. (2012). The Pan-STARRS1 Photometric System. *The Astrophysical Journal*, 750(2), 99. Retrieved from <https://iopscience.iop.org/article/10.1088/0004-637X/750/2/99/pdf>
- Wang, Xinyue (2025). Historical Data Plot Script [Python script]. GitHub. Retrieved from <https://github.com/xinyue0221/double-star-plot-scripts>
- Wenger, M. et al. (2000). The SIMBAD astronomical database. The CDS reference database for astronomical objects. *Astronomy and Astrophysics Supplement* 143, pp. 9–22. Retrieved from <astro-ph/0002110> [astro-ph]

Appendix A:

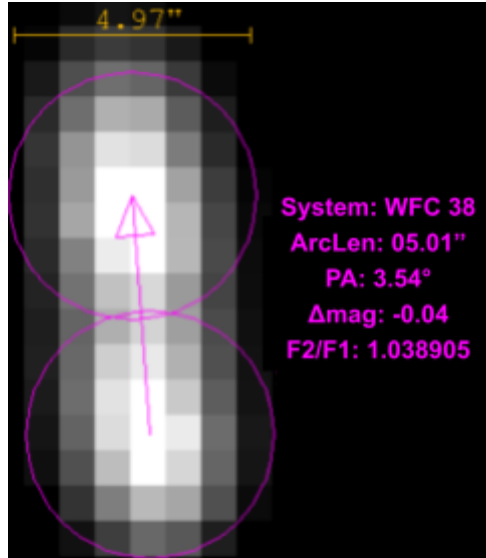


Figure A: Compromised image of the 06347-8239 WFC 38 system

Table A: Astronomical Measurements

| System | Julian Date | Image / Value | 1 | 2 | 3 | 4 | 5 | 6 | 7 | 8 | 9 | 10 | 11 |
|--------------------------------------|-------------|---------------|--------|--------|--------|--------|--------|--------|--------|--------|--------|--------|--------|
| 05276-0843 HLD 75 | 2024.019 | PA(°) | 89.207 | 89.140 | 89.099 | 89.060 | 89.081 | 89.049 | 88.994 | 89.219 | 89.108 | 89.116 | 89.134 |
| | | Sep(") | 6.270 | 6.258 | 6.258 | 6.258 | 6.306 | 6.294 | 6.270 | 6.270 | 6.264 | 6.270 | 6.264 |
| 06347-8239 WFC 38 | 2025.033 | PA(°) | 3.965 | 3.762 | 4.305 | 3.038 | 3.807 | 3.792 | 3.714 | 3.756 | 3.761 | N/A | N/A |
| | | Sep(") | 4.902 | 5.166 | 5.327 | 5.229 | 5.105 | 5.14 | 5.233 | 5.167 | 5.171 | N/A | N/A |
| 05445-2058 KPP 125 | 2025.030 | PA(°) | 154.02 | 154.20 | 154.05 | 154.29 | 153.07 | 153.49 | 153.26 | 156.05 | 154.34 | 153.32 | N/A |
| | | Sep(") | 4.83 | 4.91 | 4.93 | 4.83 | 5.05 | 5.26 | 5.15 | 5.15 | 4.90 | 4.89 | N/A |
| 10296+3757 HJ 2532 AB | 2025.038 | PA° | 69.67 | 69.73 | 69.7 | 69.79 | 69.62 | 69.51 | 69.69 | 69.73 | 69.64 | 69.74 | N/A |
| | | Sep(") | 13.00 | 12.99 | 13.02 | 13.09 | 13.03 | 13.01 | 13.02 | 13.01 | 13.07 | 13.03 | N/A |
| 09174+2339 STF 1332 (HD 79872) | 2025.041 | PA(°) | 28.586 | 29.787 | 29.07 | 29.711 | 29.192 | 29.609 | 29.804 | 30.182 | 29.834 | 30.091 | N/A |
| | | Sep(") | 5.684 | 5.973 | 5.930 | 5.921 | 5.794 | 5.966 | 5.993 | 5.982 | 5.928 | 5.844 | N/A |